Ultrafast laser-triggered field ion emission from semiconductor tip

Elena Silaeva, Angela Vella, N. Sévelin-Radiguet, G. Martel, B. Deconihout, Tatiana Itina

Ultrafast laser-triggered field ion emission from semiconductor tips

2012 New J. Phys. 14 113026

(http://iopscience.iop.org/1367-2630/14/11/113026)

New Journal of Physics
The open access journal for physics

Ultrafast laser-triggered field ion emission from semiconductor tips

E P Silaeva[1,2,3], A Vella[2], N Sevelin-Radiguet[2], G Martel[2], B Deconihout[2] and T E Itina[1]

[1] Laboratoire Hubert Curien, UMR CNRS 5516/Université Jean Monnet, 18 rue Benoît Lauras, 42000 Saint-Etienne, France
[2] Groupe de Physique des Materiaux UMR CNRS 6634, CORIA UMR 6614—UFR Sciences Site du Madrillet, Avenue de l'Université—BP 12 76801 Saint Etienne du Rouvray, France
E-mail: elena.silaeva@coria.fr

New Journal of Physics **14** (2012) 113026 (17pp)
Received 20 July 2012
Published 22 November 2012
Online at http://www.njp.org/
doi:10.1088/1367-2630/14/11/113026

Abstract. We study experimentally and theoretically the controlled field evaporation of single atoms from a semiconductor surface by ultrafast laser-assisted atom probe tomography. The conventional physical mechanisms of field evaporation cannot explain the experimental results recently reported for such materials. A new model is presented in which the positive dc field leads to band bending with a high density of laser-generated holes near the surface of the sample. The laser energy absorption by these holes and the subsequent energy transfer to the lattice considerably increase the tip temperature. We show that this heating plays an important role in the field ion emission process. In addition, experiments are carried out for germanium and silicon tips to check the role of the dc field in the absorption processes, as well as the heating of the tip and the following evaporation. Good agreement between the predictions of our model and the experimental data is found.

[3] Author to whom any correspondence should be addressed.

Contents

1. Introduction

In laser-assisted atom probe tomography (La-APT), single atoms are emitted as ions from the surface of a needle-shaped sample (a tip) one by one by the joint action of a high external dc electric field of tens of V nm^{-1} and a femtosecond laser pulse. This process is known as laser-assisted field evaporation [1–4].

For metallic tips, the conduction electrons absorb the photon energy of the laser at a very small area located close to the tip apex due to the diffraction effect related to the subwavelength dimensions of the tip [5]. These hot electrons relax their energy to the lattice and the tip temperature increases. Hence, the surface atoms are evaporated by a thermally assisted process providing a sufficiently high tip temperature [6, 7].

For semiconductor tips, the laser-assisted field evaporation mechanisms are still unclear [8–10]. Experimental three-dimensional images with atomic resolution in silicon [11] prove the surface nature of the laser-assisted field evaporation. However, in La-APT, the tip temperature is set below 80 K. At such low temperature the charge density inside a pure semiconductor is negligible and even defects, such as dopant atoms, are not fully ionized [12]. This means that the dc electric field can penetrate deep inside the sample over more than tens of nm, so that the evaporation of atoms in the form of clusters or molecular ions is expected, as was already observed for silicon by using electrical pulses [13]. Only at room temperature for doped semiconductors can the field be screened due to the presence of free charges into the bands as theoretically calculated by Tsong [14] and Ernst [15].

Clearly, in the case of La-APT analysis free charges can be generated by laser pulse, thus allowing the screening of the dc electric field. However, how does this screening process take place? To what extent and on what time scale? And, more importantly, does this process affect the optical properties of the semiconductor?

It was recently reported by Bachhav *et al* [16] that when a silicon tip is illuminated by an infrared fs laser pulse, the absorption is confined to the tip surface and the laser-assisted field evaporation takes place preferentially from the illuminated side. However, because of a rather small absorption coefficient of silicon in the infrared domain, a very small, homogeneous absorption throughout the tip volume is expected.

In this paper, a new model is presented to explain the confinement of the absorption at the tip surface. In addition, the La-APT experiments allow us to clearly demonstrate how this confinement can be affected by the presence of a high dc electric field. Changing the laser intensity, the initial temperature of the tip and the dc field applied to the tip, we experimentally

determine the increase in tip temperature at the surface after the action of a single laser pulse. These results are compared with the lattice temperature calculated numerically by taking into account the laser-induced generation of free carriers and their relaxation to the lattice. Our model is based on the drift-diffusion approach [17, 18] coupled with the classical two-temperature model [19, 20] and takes into account the band-bending effect. In particular, the calculations allow an evaluation of the laser-induced ionization, recombination effects and charge separation at the tip surface due to the dc field.

We investigate germanium (Ge) and silicon (Si) as semiconductors that are widely used in the microelectronic and photovoltaic domains. We have chosen to use infrared light (photon energy $\mathcal{E}_{\mathrm{ph}} = 1.2\,\mathrm{eV}$) to analyze a Ge tip and green light ($\mathcal{E}_{\mathrm{ph}} = 2.4\,\mathrm{eV}$) for a Si tip, in order to have the same interband absorption coefficient α^{opt}, which is equal to $10^4\,\mathrm{cm}^{-1}$ for Ge and $0.5 \times 10^4\,\mathrm{cm}^{-1}$ for Si at 77 K [21].

The paper is organized as follows. In section 2, we present our model for the laser–semiconductor interaction in the presence of a high dc electric field. First, we calculate the dynamics of band-bending accompanied by laser-induced carrier excitation. Then the heating of the tip is estimated to be a result of the laser energy absorption by the holes and energy transfer to the lattice. In section 3, our experimental results are presented and compared with the model. This leads to a new insight into the physics involved in the process. In section 4, our conclusions are presented.

2. Theoretical model

2.1. Effects of a dc electric field and femtosecond laser excitation

In the presence of a high electric field, the surface band structure of a semiconductor–vacuum interface is strongly distorted with the bands bent upward leading to high surface hole density when the applied voltage is positive [14]. However, for low temperature and before the application of the laser pulse, the free-charge density is negligible inside a pure semiconductor. The band structure is of a dielectric type with a linear voltage drop across the sample and a constant internal electric field [22]. The internal field is determined by the surface field in vacuum and the dielectric constant of a semiconductor ($\varepsilon_{\mathrm{r}} = 16.2$ for Ge and $\varepsilon_{\mathrm{r}} = 11.7$ for Si). In our model, we consider the dc field E_0 inside Ge and Si in the range of 1–3 $\mathrm{V\,nm}^{-1}$, i.e. around $E_0 = E_{\mathrm{evap}}/\varepsilon_{\mathrm{r}}$. The dc electric field allowing evaporation E_{evap} is 29 and 33 $\mathrm{V\,nm}^{-1}$ for Ge [23] and Si [24], respectively.

When a femtosecond laser pulse interacts with a semiconductor tip, it creates free carriers (free electrons and holes). The evolution of the carrier density is strongly influenced by the external dc electric field that, in turn, leads to the establishment of strong band bending at the surface. In addition, under photo-generation of electrons and holes, the equilibrium Fermi level is split into two quasi-Fermi levels.

To describe the transient response of the tip to the field during the interaction with the laser pulse, we use the drift-diffusion approach [18, 19]. In the La-APT, the laser pulse is applied perpendicularly to the main tip axis, i.e. the wave vector is perpendicular to the dc field direction of symmetry. The optical absorption depth of Ge at $\lambda = 1030\,\mathrm{nm}$ and of Si at $\lambda = 515\,\mathrm{nm}$ is $> 1\,\mu\mathrm{m}$. Far away from the hemispherical apex of the tip, the tip can be considered as a cylinder with $\sim 100\,\mathrm{nm}$ diameter, which is smaller than the optical absorption depth. Thus, the tip can be approximately described by a 1D model along its axial direction. The model consists of the

solution of the transport equations for carrier densities and the Poisson equation for the field inside the semiconductor sample as follows:

$$\begin{cases} \dfrac{\partial n_\mathrm{h}}{\partial t} - \dfrac{\partial}{\partial x}\left(D_\mathrm{h}\dfrac{\partial n_\mathrm{h}}{\partial x} + \mu_\mathrm{h} n_\mathrm{h} E\right) = S_\mathrm{h} - R_\mathrm{h}, \\ \dfrac{\partial n_\mathrm{e}}{\partial t} - \dfrac{\partial}{\partial x}\left(D_\mathrm{e}\dfrac{\partial n_\mathrm{e}}{\partial x} - \mu_\mathrm{e} n_\mathrm{e} E\right) = S_\mathrm{e} - R_\mathrm{e}, \\ \dfrac{\partial E}{\partial x} = -\dfrac{e}{\varepsilon\varepsilon_0}(n_\mathrm{h} - n_\mathrm{e}), \end{cases} \tag{1}$$

where n_h, n_e and E are the space- and time-dependent hole density, electron density and electric field, respectively, e is the absolute value of the electronic charge, and ε_0 is the electric constant.

The source of carriers, S_c (subscript c stands for either hole or electron), accounts for the interband absorption of the laser energy

$$S_\mathrm{c} = \frac{(1-\Gamma)\alpha^\mathrm{opt} I}{\mathcal{E}_\mathrm{ph}}, \tag{2}$$

where Γ is the reflectivity of the sample and I is the intensity of the laser pulse. At the given laser intensities and photon energies, multi-photon processes are negligible. For example, in Ge, the two-photon absorption cross section β is less than $10\,\mathrm{cm\,GW^{-1}}$ at 1030 nm [25]. The given intensity I is smaller than $1\,\mathrm{GW\,cm^{-2}}$, which leads to the two-photon absorption coefficient $\beta I < 10\,\mathrm{cm^{-1}}$ being much smaller than the linear absorption coefficient $\alpha_\mathrm{opt} = 10^4\,\mathrm{cm^{-1}}$.

The carrier losses in the bulk, R_c, are mainly due to the Auger recombination with coefficients of the e–h–h process $C_\mathrm{h} = 7.8 \times 10^{-32}\,\mathrm{cm^6\,s^{-1}}$ and the h–e–e process $C_\mathrm{e} = 2.3 \times 10^{-31}\,\mathrm{cm^6\,s^{-1}}$ for Si [26] and $C_\mathrm{h} = C_\mathrm{e} = 1.1 \times 10^{-31}\,\mathrm{cm^6\,s^{-1}}$ for Ge [27]

$$\begin{aligned} R_\mathrm{h} &= R_\mathrm{e} = R_\mathrm{h}^\mathrm{A} + R_\mathrm{e}^\mathrm{A}, \\ R_\mathrm{h}^\mathrm{A} &= C_\mathrm{h} n_\mathrm{h}^2 n_\mathrm{e}, \\ R_\mathrm{e}^\mathrm{A} &= C_\mathrm{e} n_\mathrm{e}^2 n_\mathrm{h}. \end{aligned} \tag{3}$$

In the transport equations, the carrier mobilities and diffusion coefficients are considered for Fermi–Dirac statistics in order to take into account degeneracy effects at high carrier densities [28]

$$\mu_\mathrm{c} = \mu_\mathrm{c}^0 \frac{\mathcal{F}_0(\eta_\mathrm{c})}{\mathcal{F}_{1/2}(\eta_\mathrm{c})}, \qquad D_\mathrm{c} = \mu_\mathrm{c}\frac{k_\mathrm{b} T_\mathrm{c}}{e}\frac{\mathcal{F}_{1/2}(\eta_\mathrm{c})}{\mathcal{F}_{-1/2}(\eta_\mathrm{c})}, \tag{4}$$

where $\mathcal{F}_\xi(\eta_\mathrm{c})$ denotes the ξth-order Fermi integral, η_c is the reduced quasi-Fermi level [29] and k_B is the Boltzmann constant. Low-density values of electron and hole mobilities at 77 K are given by $\mu_\mathrm{e}^0 = \mu_\mathrm{h}^0 = 4\,\mathrm{m^2\,(Vs)^{-1}}$ for Ge [30, 31] and $\mu_\mathrm{h}^0 = 0.92\,\mathrm{m^2\,(Vs)^{-1}}$ and $\mu_\mathrm{e}^0 = 2\,\mathrm{m^2\,(Vs)^{-1}}$ for Si [32]. The value of η_c depends on the local carrier density n_c and is calculated by the procedure described in [20]. Both the diffusion coefficient and the reduced Fermi levels depend on the carrier temperature T_c that changes during the interaction with the laser pulse. This is simultaneously calculated from the two-temperature equations described in the next subsection.

Equations (1)–(4) are solved with a finite difference method [17] together with the following initial conditions:

$$n_\mathrm{h}(x, t=0) = n_\mathrm{e}(x, t=0) = 0, \qquad E(x, t=0) = E_0, \tag{5}$$

and boundary conditions

$$
\begin{aligned}
&E(x=0,t)=E_0,\\
&D_{\mathrm{h}}\frac{\partial n_{\mathrm{h}}}{\partial x}+\mu_{\mathrm{h}}n_{\mathrm{h}}E\Big|_{x=0,t}=v_{\mathrm{sr}}n_{\mathrm{c}},\\
&D_{\mathrm{e}}\frac{\partial n_{\mathrm{e}}}{\partial x}-\mu_{\mathrm{e}}n_{\mathrm{e}}E\Big|_{x=0,t}=v_{\mathrm{sr}}n_{\mathrm{c}},\\
&D_{he}\frac{\partial n_{\mathrm{h}}}{\partial x}+\mu_{\mathrm{h}}n_{\mathrm{h}}E\Big|_{x=L,t}=D_{\mathrm{e}}\frac{\partial n_{\mathrm{e}}}{\partial x}-\mu_{\mathrm{e}}n_{\mathrm{e}}E\Big|_{x=L,t}=0,
\end{aligned}
\tag{6}
$$

where L is the length of the considered sample and v_{sr} is the surface recombination velocity. The value of v_{sr} depends on the density of surface states and for Ge and Si ranges from 10^2 to $10^6\,\mathrm{cm\,s^{-1}}$ [33–35]. The surface-recombination rate is limited by the surface minority carriers. Thus, in equation (6) $n_{\mathrm{c}}=n_{\mathrm{e}}$ if there are fewer electrons than holes and $n_{\mathrm{c}}=n_{\mathrm{h}}$ in the opposite case.

The boundary conditions (6) for electron and hole currents are chosen to maintain the conservation of particles, i.e. no charge carriers leave either the left ($x=0$) or the right boundary ($x=L$). The left boundary condition for the dc field E ($x=0$) is kept constant. In the numerical solution, the sample is divided into layers (numerical cells) with variable thickness. The first numerical cell at the sample surface is 10^{-10} m, increasing to the bulk. Because of the very high field and, thus, carrier drift velocity the time step is required to be very small, 10^{-20} s, so the calculations are time-consuming. Therefore, we focus our attention only on several picoseconds after the beginning of the laser pulse.

We consider the Gaussian temporal profile with the pulse width (full-width at half-maximum (FWHM)) $\tau_{\mathrm{p}}=500\,\mathrm{fs}$, the peak intensity of $1\,\mathrm{GW\,cm^{-2}}$, laser wavelength $\lambda=1030\,\mathrm{nm}$ for Ge and $\lambda=515\,\mathrm{nm}$ for Si. The size of the sample is taken as $L=20\,\mu\mathrm{m}$. It is assumed that the lasing starts at $t=0$, reaches the maximum intensity at $t=600\,\mathrm{fs}$ and ends at $t=1200\,\mathrm{fs}$.

In the presence of a positive external dc field, the photo-generated holes start drifting toward the surface, whereas the electrons drift in the opposite direction. This effect leads to a significant increase in the hole density at the surface with respect to its bulk value (figure 1(a)). The separation of holes from electrons generates space charge that results in the screening of the external field. During the laser pulse, the dc field gradually decreases in the bulk (figure 1(b)). When the carrier distributions reach a quasi-equilibrium governed by the balance between drift and diffusion currents, the field becomes completely screened ($t\simeq 1\,\mathrm{ps}$). By this time, the valence band maximum at the surface is significantly higher than the hole quasi-Fermi level in the bulk and the hole density reaches $n_{\mathrm{h}}\simeq 2.7\times10^{21}\,\mathrm{cm^{-3}}$ for Ge for $E_0=1.5\,\mathrm{V\,nm^{-1}}$. For Si, the charge movement and field screening evolve similarly with the maximum hole density $n_{\mathrm{h}}\simeq 3.2\times10^{21}\,\mathrm{cm^{-3}}$ for $E_0=2\,\mathrm{V\,nm^{-1}}$ (due to the similarity, the corresponding figures were not shown). Therefore, these holes will significantly absorb the laser energy at the surface. The free-carrier absorption is related to the change of the complex dielectric function $\Delta\varepsilon^{\mathrm{fcr}}$, which depends on the carrier density and laser wavelength according to the Drude model [36]

$$
\begin{aligned}
\Delta\varepsilon^{\mathrm{fcr}}&=\Delta\varepsilon_{\mathrm{e}}^{\mathrm{fcr}}+\Delta\varepsilon_{\mathrm{h}}^{\mathrm{fcr}},\\
\Delta\varepsilon_{\mathrm{c}}^{\mathrm{fcr}}&=-\frac{n_{\mathrm{c}}e^2}{\varepsilon_0 m_{\mathrm{c}}^{*}\omega^2}\frac{1}{1+\mathrm{i}(\omega\tau_{\mathrm{D}})^{-1}},
\end{aligned}
\tag{7}
$$

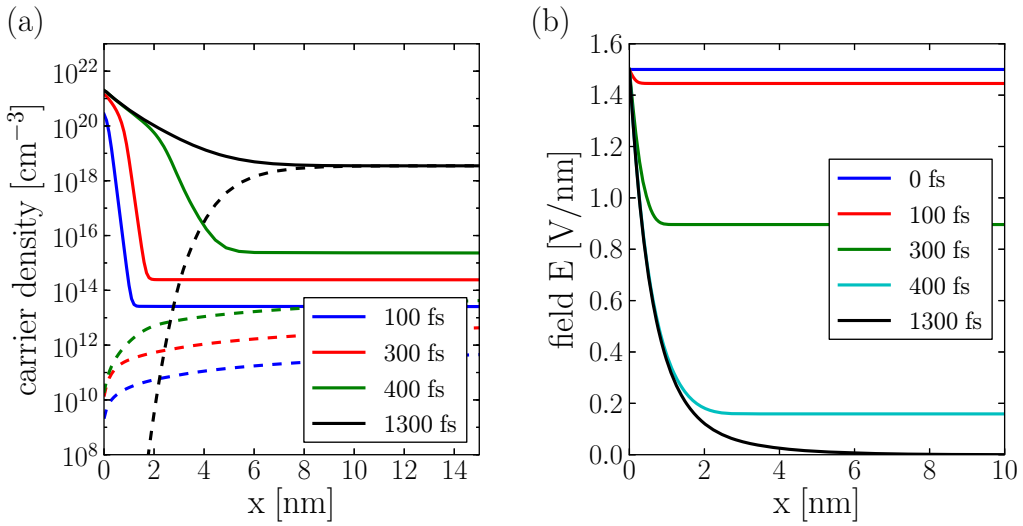

Figure 1. Spatial profiles inside the Ge sample at different times for (a) hole density (solid lines) and electron density (dashed lines) and (b) dc electric field. $x = 0$ corresponds to the surface of the sample. Laser pulse parameters: $I = 1\,\mathrm{GW\,cm^{-2}}$, $\tau_\mathrm{p} = 500\,\mathrm{fs}$, the pulse peak at 600 fs. The external dc field at the surface $E_0 = 1.5\,\mathrm{V\,nm^{-1}}$. The surface recombination velocity $v_\mathrm{sr} = 10^6\,\mathrm{cm\,s^{-1}}$.

where τ_D is the carrier damping time and $\omega = 2\pi c/\lambda$ is the laser frequency. For Ge, the carrier effective masses m_c^* are taken as $m_\mathrm{h}^* = 0.23m_\mathrm{e}$ and $m_\mathrm{e}^* = 0.12m_\mathrm{e}$ [34] and for Si $m_\mathrm{h}^* = m_\mathrm{e}^* = 0.5m_\mathrm{e}$ [33]. The free-carrier absorption coefficient is given by

$$\alpha_\mathrm{c}^\mathrm{fcr} = \frac{4\pi}{\lambda\sqrt{2}}([\mathrm{Re}^2\Delta\varepsilon_\mathrm{c}^\mathrm{fcr} + \mathrm{Im}^2\Delta\varepsilon_\mathrm{c}^\mathrm{fcr}]^{1/2} - \mathrm{Re}\Delta\varepsilon_\mathrm{c}^\mathrm{fcr})^{1/2}. \tag{8}$$

The value of $\alpha_\mathrm{h}^\mathrm{fcr}$ is about $10^5\,\mathrm{cm^{-1}}$ for both Ge and Si at the surface when early during the laser pulse the hole density reaches more than $10^{21}\,\mathrm{cm^{-3}}$ due to the band bending. This value is almost ten times higher than the interband absorption coefficients of Ge and Si at 80 K for infrared and green light, respectively, showing that under a high electric field the optical properties of the surface of the sample are changed following the dynamics of the spatial distribution of charges. Note that we also take into account a change of the sample reflectivity Γ according to the modified dielectric function (equation (7)).

The carrier damping time τ_D in equation (7) depends on many processes, such as carrier–phonon collisions, carrier–carrier collisions, degeneracy of carrier distribution and surface roughness scattering [37, 38]. It becomes very short at high carrier densities. The value of about 1 fs is reported for optically excited silicon [18, 36]. At low densities, however, it can be 100 times longer. We take $\tau_\mathrm{D} = 1\,\mathrm{fs}$ as hole and electron damping time everywhere in the sample, for simplicity. In the regions of low density of holes, i.e. bulk of the sample, the free-carrier absorption is much lower than interband absorption and does not significantly contribute to the total absorption. The density of the electrons and free-electron absorption is low in the bulk, as well as at the surface.

2.2. Surface temperature

The temperature of the surface of the tip is determined by the processes of tip heating and heat dissipation in the bulk. The heating of the semiconductor material by the laser pulse is caused by the transfer of energy from the carriers to the lattice through carrier–phonon coupling and carrier recombination.

The excess energy $\mathcal{E}_c$ of a created electron–hole pair depends on the photon energy and band gap of the material. It gives to carriers the initial kinetic energy and leads to the elevated initial carrier temperature. The carriers thermalize then into Fermi–Dirac distribution via carrier–carrier collisions on a femtosecond time scale. Hence, the total kinetic energy density in the carrier system is given as [19]

$$\mathcal{E}_c n_c = \frac{3}{2} n_c k_B T_c \frac{\mathcal{F}_{3/2}(\eta_c)}{\mathcal{F}_{1/2}(\eta_c)}. \tag{9}$$

The excess energy is divided between a hole and an electron according to their effective masses. For Ge at infrared excitation and band gap $\mathcal{E}_g = 0.73\,\text{eV}$ at 80 K the excess hole energy is equal to $\mathcal{E}_h \frac{m_h^*}{m_h^*+m_e^*}(\mathcal{E}_{ph} - \mathcal{E}_g) \sim 0.31\,\text{eV}$. From equation (9), it follows that the initial hot-hole temperature $T_{h0} \simeq 2420\,\text{K}$. Similarly, the initial hot-electron temperature is $T_{e0} \simeq 1250\,\text{K}$. For Si at green light excitation ($\mathcal{E}_g = 1.15\,\text{eV}$) the excess energy is $\mathcal{E}_h = \mathcal{E}_{h0} \simeq 0.6\,\text{eV}$ and the hot-hole and hot-electron temperature is $T_{h0} = T_{e0} \simeq 4640\,\text{K}$. The additional kinetic energy is provided through free-carrier absorption to electrons and holes. During the Auger recombination process, two carriers recombine and a third carrier takes a part of the total energy, corresponding to the sum of kinetic energies and band gap. Thus, Auger recombination reduces the carrier number, while increasing the carrier temperature.

Several effects can lead to different energies of electron and hole subsystems and, thus, energy exchange between them. However, as shown in the previous subsection, in the bulk of the sample the dc field is screened, thus an electron–hole pair behaves like one particle and only its total energy is important. At the surface, the holes and electrons are separated and cannot interact. This allows us to neglect the electron–hole energy exchange in the calculations.

We note that because of surface defects, the band gap of a semiconductor can be lower at the surface than in the bulk [39], which can lead in turn to higher excess energy and higher generation rate of the carriers at the surface. However, as shown above, the value of the hole density at the surface is determined by the applied dc field and average density of the holes inside the sample (figure 1(a)). The additional increase in carrier number in a small near-surface region would not change this process significantly. Thus, we fix the band gap at the constant along the sample.

Furthermore, we neglect the effect of carrier heating by the dc field. To acquire some energy from the dc field, the carriers need to travel a sufficient distance. However, they are just slightly and rapidly redistributed under the dc field here. When quasi-equilibrium is reached, the carriers do not drift anymore. This fact also means that we can neglect the possible carrier energy loss through the impact ionization process. For this process to have a higher rate than energy loss through carrier–phonon coupling, the energy of a carrier has to be in excess of $1.5\mathcal{E}_g$ [40]. In the considered case, the excess energy of a carrier is below $1.5\mathcal{E}_g$. Also, the impact ionization rate is diminished at the surface, where only holes are present.

The temperature of the holes T_h, electrons T_e and lattice T_L are then calculated separately by using the following equations [20]:

$$\begin{cases} \dfrac{\partial}{\partial t}(C_h T_h) = S_h \dfrac{m_h^*}{m_h^* + m_e^*}(\mathcal{E}_{ph} - \mathcal{E}_g) + \mathcal{E}_g R_h^A + (1-\Gamma)\alpha_h^{fcr} I - \dfrac{C_h}{\tau_{ph}}(T_h - T_L) + \dfrac{\partial}{\partial x} K_h \dfrac{\partial T_h}{\partial x}, \\ \dfrac{\partial}{\partial t}(C_e T_e) = S_e \dfrac{m_e^*}{m_h^* + m_e^*}(\mathcal{E}_{ph} - \mathcal{E}_g) + \mathcal{E}_g R_e^A + (1-\Gamma)\alpha_e^{fcr} I - \dfrac{C_e}{\tau_{ph}}(T_e - T_L) + \dfrac{\partial}{\partial x} K_e \dfrac{\partial T_e}{\partial x}, \\ \dfrac{\partial}{\partial t}(C_L T_L) = \dfrac{C_h}{\tau_{ph}}(T_h - T_L) + \dfrac{C_e}{\tau_{ph}}(T_e - T_L) + \dfrac{\partial}{\partial x} K_L \dfrac{\partial T_L}{\partial x}. \end{cases} \tag{10}$$

The coefficient C_c describes the heat capacity of the carrier system and is given as [20]

$$C_c = \frac{3}{2} n_c k_B \left\{ \frac{\mathcal{F}_{3/2}(\eta_c)}{\mathcal{F}_{1/2}(\eta_c)} - \eta_c \left[1 - \frac{\mathcal{F}_{3/2}(\eta_c)\mathcal{F}_{-1/2}(\eta_c)}{\mathcal{F}_{1/2}(\eta_c)^2} \right] \right\}. \tag{11}$$

The thermal conductivity of carriers is taken as [20]

$$K_c = \frac{k_B^2 n_c \mu_c T_c}{e} \left(6\frac{\mathcal{F}_2(\eta_c)}{\mathcal{F}_0(\eta_c)} - 4\frac{\mathcal{F}_1(\eta_c)^2}{\mathcal{F}_0(\eta_c)^2} \right). \tag{12}$$

The lattice heat capacity C_L strongly depends on lattice temperature below 300 K [41], as well as thermal conductivity K_L that is reported in the literature for Ge and Si nanowires, whose geometry is close to the APT tip geometry [42]. These dependences are taken into account in the model.

The electron and hole energy coupling to the lattice is described by the carrier–phonon energy relaxation time τ_{ph}, determined by optical- and acoustic-phonon scattering. This process is known to be different for electrons and holes in Ge and Si [43] and depends in a complicated way on carrier density, carrier temperature and lattice temperature [44, 45]. Also, the peculiarity of the given configuration with the electron–hole separation and a very thin layer of the high-density hole gas can additionally influence the process of energy coupling. Because of such an uncertainty in the exact value of τ_{ph}, we approximate it to be constant and the same for the electrons and holes, following the reported empirical values of 300 fs for Ge and 240 fs for Si [18, 19, 34].

The initial and boundary conditions for the temperatures are as follows:

$$\begin{aligned} &T_h(x, t=0) = T_{h0}, \quad T_e(x, t=0) = T_{e0}, \\ &T_L(x, t=0) = 80\ \text{K}, \end{aligned} \tag{13}$$

$$\begin{aligned} &\left.\frac{\partial T_h}{\partial x}\right|_{x=0,t} = \left.\frac{\partial T_e}{\partial x}\right|_{x=0,t} = 0, \\ &K_L \left.\frac{\partial T_L}{\partial x}\right|_{x=0,t} = -v_{sr} n_c \mathcal{E}_g, \\ &T_h = T_e = T_L = 80\ \text{K} \ \text{ at } x = L. \end{aligned} \tag{14}$$

Because there are no carriers before the application of the laser pulse, the initial condition for the carrier temperature means that when the first carriers are created they have temperature equal to T_{c0}. The boundary conditions for the carrier temperature are adiabatic at $x = 0$. The value

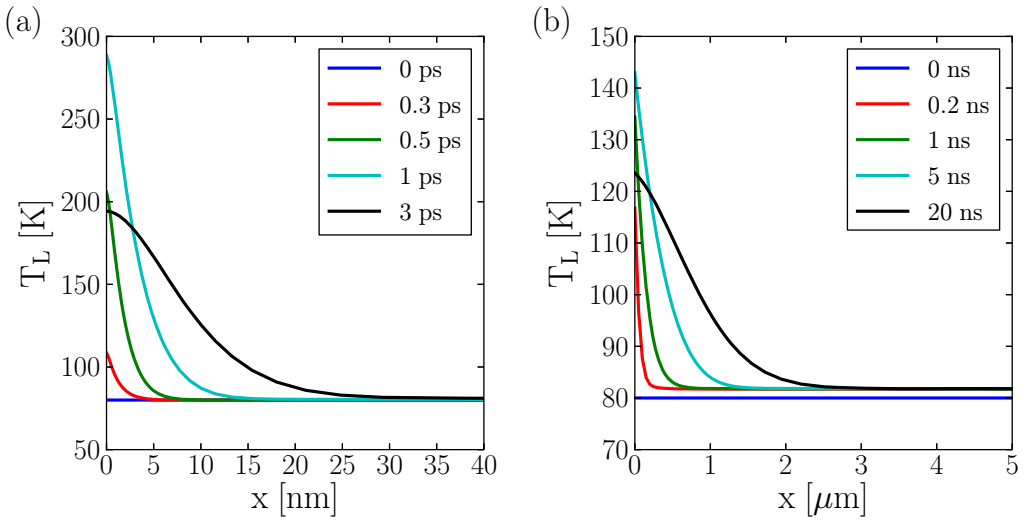

Figure 2. Spatial distributions of lattice temperature for a Ge sample at different times (a) with dc field $E_0 = 1.5\,\mathrm{V\,nm^{-1}}$ and (b) without dc field $x = 0$ corresponds to the surface of the sample. The surface recombination velocity is $v_{sr} = 10^6\,\mathrm{cm\,s^{-1}}$. Laser pulse parameters: $I = 1\,\mathrm{GW\,cm^{-2}}$, $\tau_p = 500\,\mathrm{fs}$, the pulse peak at 600 fs.

of T_L at $x = 0$ depends on the surface-recombination rate. In this process, the energy $\mathcal{E}_g$ per electron–hole pair is absorbed directly by the lattice via multi-phonon emission [33]. At $x = L$ the carrier and lattice temperature is kept at 80 K.

The self-consistent numerical solution of equations (10)–(12) together with equations (1)–(4) and boundary conditions (5), (6) (13) and(14) gives the change of the lattice temperature in space and time. The surface recombination becomes negligible and temporal evolution of the temperature is determined by the thermalization process between the hot holes and the lattice, because of the field-induced charge separation and very low density of electrons at the surface [46]. The lattice temperature is determined mostly by the density of holes, their initial temperature and temperature increase due to the free-carrier absorption effect. Thus, the tip temperature at the surface is higher than in the bulk due to the substantially higher surface hole density (figure 2(a)). At $1\,\mathrm{GW\,cm^{-2}}$ laser intensity, the surface temperature reaches $T_L \simeq 285\,\mathrm{K}$ for Ge at $E_0 = 1.5\,\mathrm{V\,nm^{-1}}$ and $T_L \simeq 270\,\mathrm{K}$ for Si at $E_0 = 2\,\mathrm{V\,nm^{-1}}$ (figure 3(a)).

For comparison, we performed the same calculations for Ge at zero dc field. In this case, the thermalization of the hot carriers with lattice leads to a small increase in average temperature along the whole sample because of the relatively low carrier density. The charge separation does not take place in the absence of the field and surface heating is determined solely by the surface recombination process (figure 2(b)). At $1\,\mathrm{GW\,cm^{-2}}$ laser pulse intensity and for the lowest reported value of surface recombination velocity, the temperature rise at the surface is 3 K, whereas for the highest it is 63 K (figure 3(b)). In both cases the surface temperature rise is substantially lower than that in the presence of the high dc field $E_0 = 1.5\,\mathrm{V\,nm^{-1}}$ and holes accumulation (205 K). We also note that the tip heating and cooling is a much longer process in the case of zero field.

Moreover, the surface peak temperature is calculated as a function of laser intensity for different dc electric fields. The results are presented in figure 4. The surface temperature

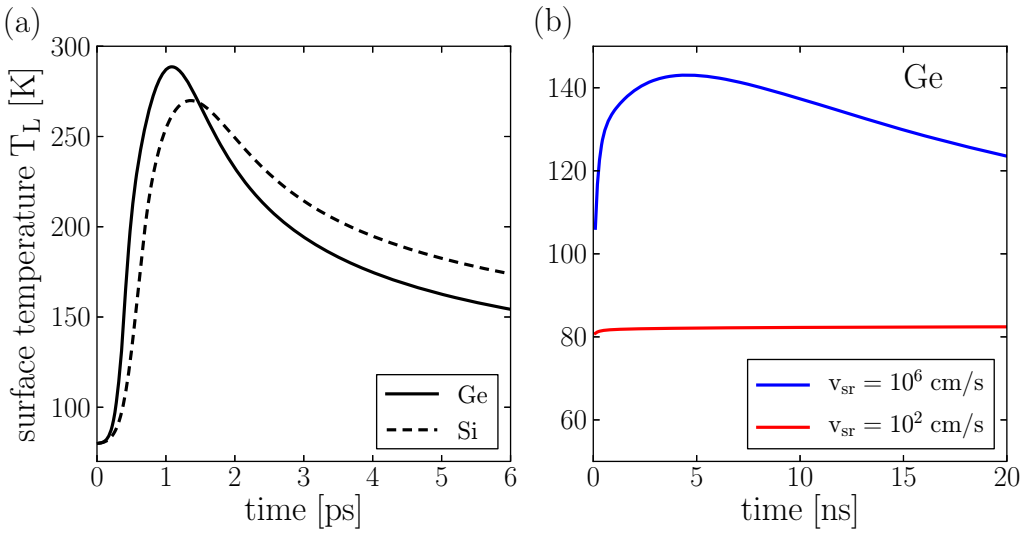

Figure 3. Lattice temperature at the surface $T_L(x = 0)$ as a function of time (a) with a dc field $E_0 = 1.5\,\mathrm{V\,m^{-1}}$ for the Ge sample and $E_0 = 2\,\mathrm{V\,nm^{-1}}$ for Si; (b) without a dc field for the Ge sample for different values of surface recombination velocity v_{sr}.

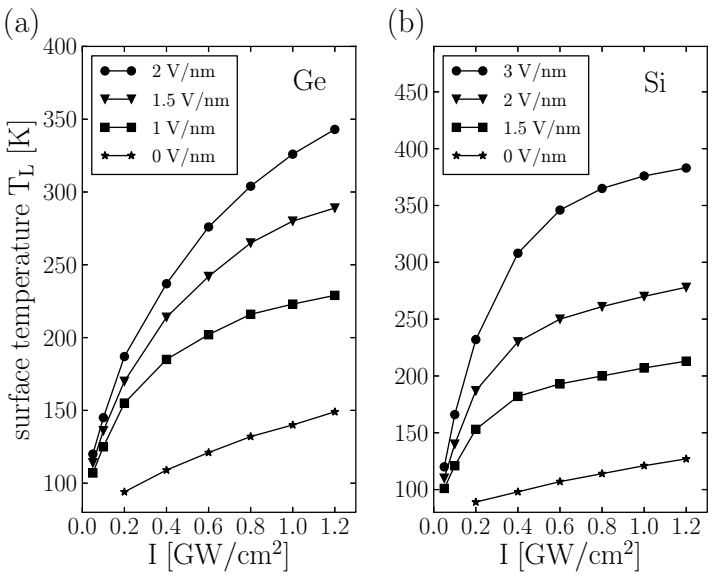

Figure 4. Surface peak temperature of Ge (a) and Si (b) samples as a function of laser pulse intensity at different values of dc field E_0. Pulse width $\tau_p = 500\,\mathrm{fs}$ and the surface recombination velocity $v_{sr} = 10^6\,\mathrm{cm\,s^{-1}}$.

increases with laser intensity due to the increase in both the absorbed energy by holes and the hole density at the surface during the laser pulse. However, the hole density is limited by the maximum band bending at the given field, determined by the stationary solution of the Poisson equation [14]. When this maximum possible hole density is reached at the surface early during the laser pulse, the additional increase of intensity does not lead to a significant

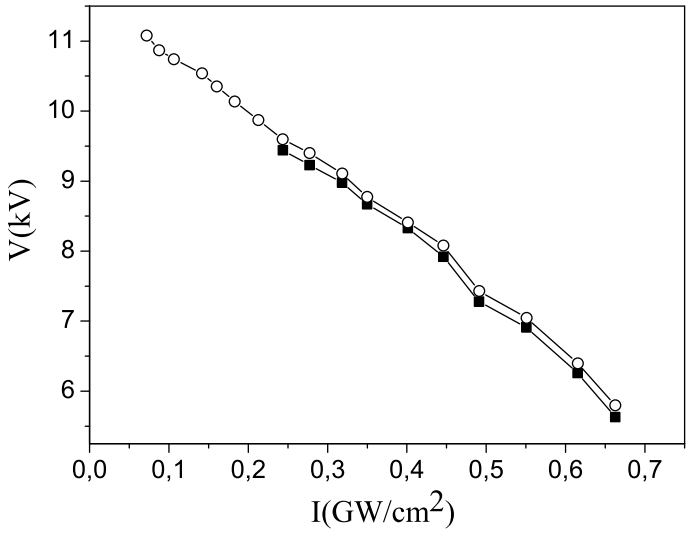

Figure 5. The dc voltage as a function of the laser intensity at 2×10^{-3} detected atoms per pulse for a tungsten tip. Full squares correspond to the data collected for a base temperature of 80 K and open dots correspond to a base temperature of 20 K.

increase of temperature. In addition, the heat capacity is higher at higher temperature; thus much more energy is needed to additionally increase the sample temperature. This leads to the much slower increase of surface temperature at higher laser intensities, showing a tendency towards saturation. At lower dc field the maximum hole density at the surface is lower, leading to a lower surface temperature. One can note that for the same dc field applied to Ge and Si samples the maximum temperature of Si is lower. This can be attributed to the lower hole mobility and higher thermal conductivity of Si with respect to Ge.

3. Experimental results

In our experiments, we use a 100 kHz pulsed ytterbium-doped laser ($\lambda = 1030$ nm) with 500 fs pulse duration and a tunable energy of up to 10 μJ per pulse to illuminate the Ge tip. The sample is placed in the ultra-high vacuum ($<10^{-7}$ Pa) chamber of an La-APT with a flight path of about 10 cm [3]. A position-sensitive detector [47] with improved multi-hit capabilities is used to accurately measure the detection rate as a function of the dc field on the sample and the laser intensity. The laser beam is slightly focused onto the tip with a spot diameter of 100 μm at FWHM controlled by a CCD camera [3]. We use a nonlinear crystal to change the laser wavelength to the green spectral region ($\lambda = 515$ nm) with a spot diameter of 40 μm to analyze the Si tip. The samples are prepared in the form of a tip by the focused ion beam milling technique [48].

The sample temperature is set equal to 80 K. Then, for a given value of the laser intensity, the dc voltage applied to the tip is adjusted to evaporate 2×10^{-3} atoms per pulse. The same procedure is repeated for each value of the laser intensity reported in figures 5 and 6. For a

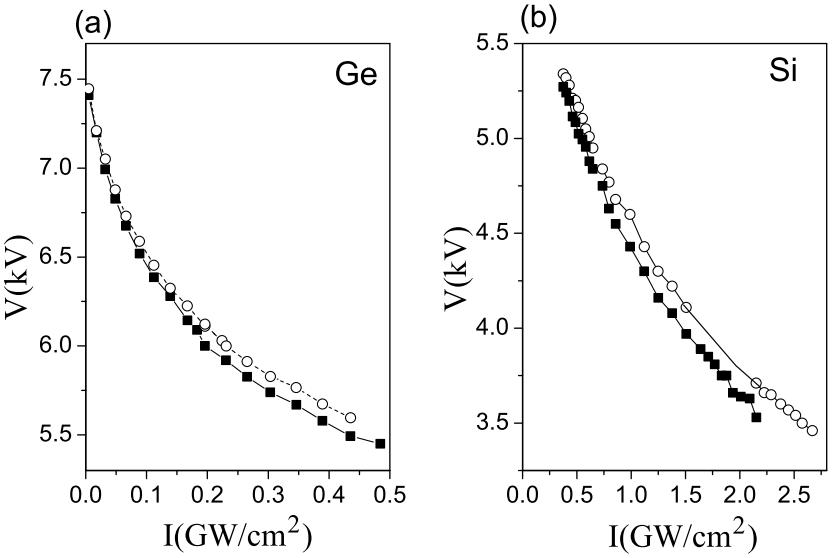

Figure 6. The dc voltage as a function of the laser intensity at 2×10^{-3} detected atoms per pulse for (a) the Ge tip and (b) the Si tip. Full squares correspond to the data collected for a base temperature of 80 K and open dots correspond to a base temperature of 20 K.

thermally assisted evaporation, the evaporation rate follows an Arrhenius law [2]

$$\varphi = \nu \langle N_k \rangle \exp\left(-\frac{Q_n}{k_B T}\right), \tag{15}$$

where ν is the surface vibration frequency, $\langle N_k \rangle$ is the number of kink site atoms within the field of view of the detector, Q_n is the activation barrier and T is the tip temperature at the surface. The number of evaporated atoms per pulse is linearly related to the evaporation rate

$$N = \varphi \tau_{\text{evap}}, \tag{16}$$

where τ_{evap} is the evaporation time for one pulse. The tip temperature depends on the laser intensity as follows:

$$T = T_0 + \delta I \tag{17}$$

with T_0 the tip base temperature and δ a proportionality factor. The activation barrier is a complex function of the field but in a first approximation it is linearly dependent on the dc field [49]

$$Q_n = Q_0' \left(1 - \frac{E}{E_{\text{evap}}}\right) \tag{18}$$

with Q_0' a proportionality factor resulting from the linearization of $Q_n(E)$ with E. The field E at the tip surface is controlled by the applied voltage V according to the relation

$$E = \frac{V}{\kappa R_{\text{tip}}}, \tag{19}$$

where $R_{\text{tip}} = (50 \pm 5)$ nm is the tip apex radius of curvature and κ is a dimensionless factor that varies with the exact geometry of the tip, which is found in the range of 2–8. In La-APT, the voltage is adjusted to have dc field values in the range of 70–95% of E_{evap}.

From equations (15)–(19), for a constant evaporation rate φ, the voltage applied to the sample becomes a linear function of the laser intensity

$$\frac{V}{V_{\text{evap}}} = 1 - \frac{\ln(\varphi) - \ln(\nu\langle N_k\rangle)}{Q_0'}(\delta I + T_0). \tag{20}$$

This linear behavior has already been reported for metals [50]. It is shown for a large range of laser intensities in figure 5 for a tungsten tip.

In the case of germanium and silicon, however, this dependence is not linear and, for high laser intensity, the laser contribution to the evaporation tends to saturate. As discussed in the first section, this result is related to the decrease of the dc voltage. For the same value of the laser intensity focused on the sample, in the case of lower voltage (and, thus, field) the lattice temperature will be lower, as shown in figure 4. Therefore, to evaporate the sample, a much higher intensity is required.

The change in base temperature from 80 to 20 K does not affect the behavior of dc voltage as a function of the laser intensity as shown in figure 6. However, for a given laser intensity the dc voltage, required to obtain a fixed number of evaporated atoms, is now higher. The difference in dc voltage values measured at 80 and 20 K is almost constant for all the values of laser intensity, because it is only related to the difference in the base temperature, which is constant and equal to 60 K.

For a fixed dc voltage, furthermore, the same number of evaporated atoms is obtained for two different values of the laser intensity: the higher value corresponds to the lower base temperature of 20 K. The intensity difference ΔI gives directly the value of the laser intensity necessary for increasing the base temperature of the sample from 20 to 80 K. From the energy conservation law,

$$\int_{20}^{80} C_{\text{L}}(T)\,\mathrm{d}T = \eta \Delta I, \tag{21}$$

where the left side describes the energy stored in the system due to the increase of the base temperature and the right side the absorbed laser energy. The η factor is related to the sample absorption coefficient and provides information about the laser efficiency in the field evaporation process. As shown in figure 5, the value of η is constant for all the values of the dc voltage for the tungsten tip, as expected for metal samples, because ΔI is constant. In fact, in the case of metals the field is screened at the surface; therefore the dependence of the optical properties on the field has never been reported. For germanium and silicon, however, when the dc voltage decreases, the η factor decreases too. This shows that the laser efficiency in the evaporation process strongly depends on the dc field applied to the sample for semiconductors. These results are in agreement with the prediction of our model showing that the surface optical properties of semiconductors change strongly under the high dc field. Thus, the increase of the lattice temperature after the free-charge relaxation depends strongly on the dc field.

To demonstrate the dependence of the laser efficiency on the dc field, we keep constant the dc voltage applied to the sample at $V = 5.5$ kV for Ge and $V = 5$ kV for Si and we increase the laser intensity focused on the sample, in order to observe the evaporation rate behavior as predicted by our theoretical model. The number of the evaporated atoms per pulse measured for the two base temperatures of 20 and 80 K as a function of the laser intensity is reported in figure 7. For a low evaporation rate ($N < 10^{-3}$ atom per pulse) Si is known to be strongly sensitive to the presence of residual hydrogen in the chamber [2]. In addition, at low laser intensity, evaporation mechanisms different from the thermally assisted evaporation take place

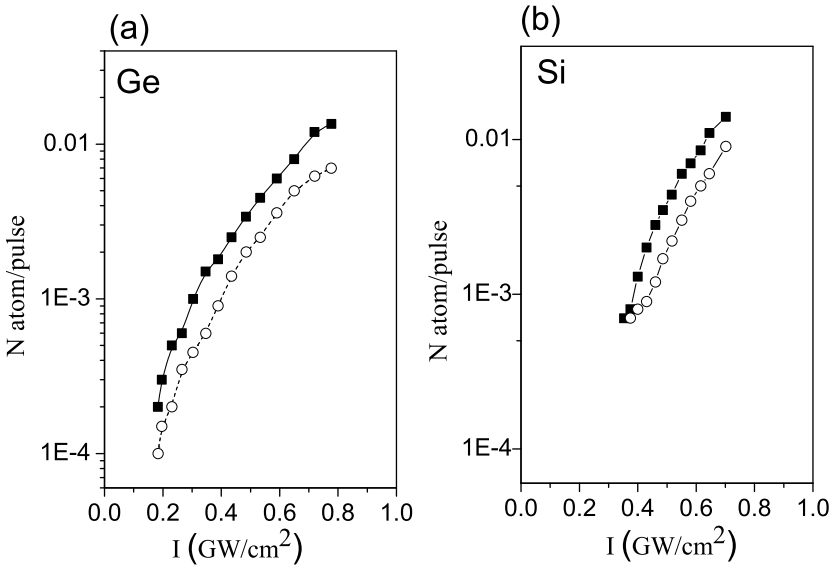

Figure 7. The number of detected atoms per pulse as a function of laser intensity for (a) the Ge tip and (b) the Si tip. Full squares correspond to the data collected for a base temperature of 80 K and open dots correspond to a base temperature of 20 K.

in the case of Si [9, 51]. For this reason, the Si sample was analyzed at a higher evaporation rate with respect to Ge.

In figure 7, we again observe that a higher laser intensity is required for evaporating the sample at lower base temperature. Thus, we can calculate the η factor and observe that η is a function of the evaporation rate. At a high evaporation rate, the η factor is smaller, corresponding to a smaller efficiency of the laser in the evaporation process. As predicted by our model, the decrease of the laser efficiency is related to the saturation of hole density at higher intensities and the increase of the semiconductor heat capacity with temperature.

By using the values of η obtained from the data reported in figure 7, we can calculate the temperature of the tip surface corresponding to the lattice temperature of our model

$$\int_{80}^{T_L} C_L(T)\,dT = \eta I. \tag{22}$$

The values of the temperature are reported in figure 8 as a function of the laser intensity. The voltage used to obtain these results approximately corresponds to dc field between 1 and 1.5 V nm^{-1} inside Ge and between 1.5 and 2 V nm^{-1} inside Si. The electric field values are estimated by using the charge state distribution derived by Kingham [52]. We can observe that the values of the temperature obtained experimentally are in the same range as the values theoretically calculated and reported in figure 4. We note that for the values of the intensity used in our experiments, we can explore only the beginning of the saturation region. When the evaporation rate is too high ($N > 0.04$ atom per pulse), our detection system requires a change of the laser repetition rate. The evaporation rate becomes unstable at 100 kHz, which can affect the thermalization of our sample and thus the experimental results.

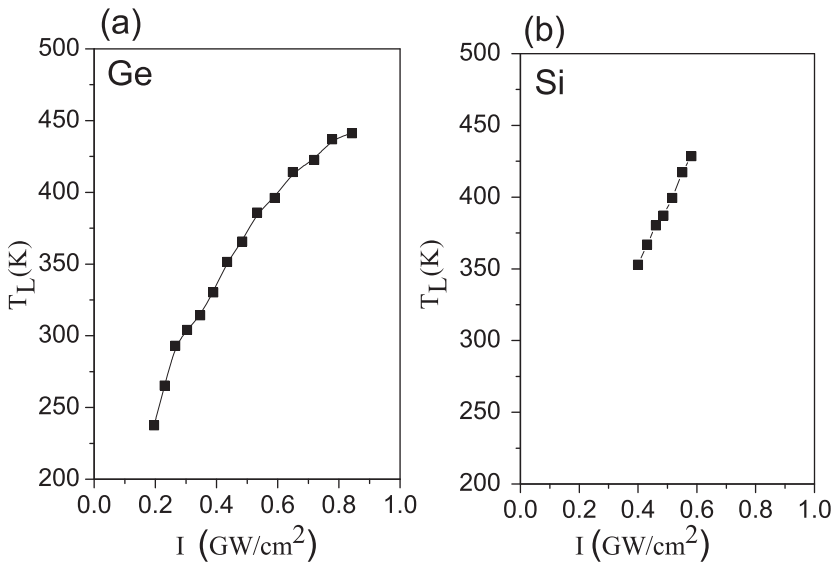

Figure 8. Temperature of the tip as a function of the laser intensity for a fixed voltage V. (a) the Ge tip, $V = 5.5$ kV; (b) the Si tip, $V = 5$ kV.

4. Conclusion

We have studied the femtosecond laser-assisted field evaporation of germanium and silicon tips at different values of the dc electric field and laser pulse energy. It has been shown experimentally that the efficiency of the laser pulse depends on the dc field for the semiconductor tip, in comparison with the metallic sample where this dependence is not observed.

The developed theoretical model has demonstrated that the dc field leads to strong band-bending and separation of the laser-generated electrons from the holes with the accumulation of the latter carriers at the apex of the semiconductor tip. The density of the holes and their temperature at the surface are high enough to sufficiently heat the lattice and provide the experimentally observed evaporation rate. The temperature rise of the lattice obtained for a high dc field is found to be significantly higher than in the absence of the field. This effect makes it possible to successfully analyze semiconductor materials by the La-APT.

La-APT is also shown to be a promising experimental method for the study of laser–matter interaction. In the considered case, it can serve as a tool for probing carrier density in the space-charge layer of semiconductors and field-induced free-carrier absorption.

We note that sample geometry can affect the tip response to laser irradiation [7]. The results presented here have shown, however, that the developed one-dimensional model gives a rather good qualitative explanation of the experimental observations.

The analysis performed sheds light on puzzling questions concerning the mechanisms of ion emission in La-APT of semiconductors and can be used to explain a wide variety of experiments in this field. In addition, the results help us to elucidate the mechanism of ultrafast laser interactions under many other similar conditions such as those in microelectronics and atomic force microscopy.

Acknowledgment

We gratefully acknowledge financial support from the ANR Ultra-Sonde 2010 BLAN 0943 01 project and computer support from the CINES of France under the project c20122085015.

References

[1] Blavette D, Bostel A, Sarrau J M, Deconihout B and Menand A 1993 *Nature* **363** 432
[2] Miller M K, Cerezo A, Hetherington M G and Smith G D W 1996 *Atom Probe Field Ion Microscopy* (Oxford: Oxford Science Publications)
[3] Gault B, Vurpillot F, Vella A, Bostel A, Menand A and Deconihout B 2006 *Rev. Sci. Instrum.* **77** 043705
[4] Kelly T F and Miller M K 2007 *Rev. Sci. Instrum.* **78** 31101
[5] Houard J, Vella A, Vurpillot F and Deconihout B 2010 *Phys. Rev.* B **81** 125411
[6] Cerezo A, Smith G D W and Clifton P H 2006 *Appl. Phys. Lett.* **88** 154103
[7] Houard J, Vella A, Vurpillot F and Deconihout B 2011 *Phys. Rev.* B **84** 033405
[8] Mazumder B, Vella A, Vurpillot F, Martel G and Deconihout B 2010 *Appl. Phys. Lett.* **97** 073104
[9] Mazumder B, Vella A, Gilbert M, Deconihout B and Schmitz G 2010 *New J. Phys.* **12** 113029
[10] Koelling S, Innocenti N, Schulze A, Gilbert M, Kambham A and Vandervorst W 2011 *J. Appl. Phys.* **109** 104909
[11] Cadel E, Vurpillot F, Lardé R, Duguay S and Deconihout B 2009 *J. Appl. Phys.* **106** 044908
[12] Sproul A B and Green M A 1993 *J. Appl. Phys.* **73** 1214
[13] Liu H M, Tsong T T and Liou Y 1987 *Phys. Rev. Lett.* **58** 1535
[14] Tsong T T 1979 *Surf. Sci.* **81** 28
[15] Ernst L 1979 *Surf. Sci.* **85** 302
[16] Bachhav M, Danoix R, Vurpillot F, Hannoyer B, Ogale S and Danoix F 2011 *Appl. Phys. Lett.* **99** 084101
[17] Vasileska D and Goodnick S M 2006 *Computational Electronics* (San Francisco, CA: Morgan and Claypool)
[18] Bulgakova N M, Stoian R, Rosenfeld A, Hertel I V and Campbell E E B 2004 *Phys. Rev.* B **69** 054102
[19] van Driel H M 1987 *Phys. Rev.* B **35** 8166
[20] Chen J K, Tzou D Y and Beraun J E 2005 *Int. J. Heat Mass Transfer* **48** 501
[21] Dash W C and Newman R 1955 *Phys. Rev.* **99** 1151
[22] Oberdorfer C and Schmitz G 2011 *Microsc. Microanal.* **17** 15
[23] Miller M K and Smith G D W 1989 *Atom Probe Microanalysis: Principles and Applications to Materials Problems* (Pittsburgh, PA: Materials Research Society)
[24] Kellogg G L 1983 *Phys. Rev.* B **28** 1957
[25] Garcia H and Avanaki K N *Appl. Phys. Lett.* **100** 131105
[26] Dziewior J and Schmid W 1977 *Appl. Phys. Lett.* **31** 346
[27] Auston D H, Shank C V and LeFur P 1975 *Phys. Rev. Lett.* **35** 1022
[28] Jungel A, Krause S and Pietra P 2011 *Z. Angew. Math. Phys.* **62** 623
[29] Sze S M and Ng K K 1969 *Physics of Semiconductor Devices* (New York: Wiley-Interscience)
[30] Jacoboni C, Nava F, Canali C and Ottaviani G 1981 *Phys. Rev.* B **24** 1014
[31] Reggiani L, Canali C, Nava F and Ottaviani G 1977 *Phys. Rev.* B **16** 2781
[32] Omar M A and Reggiani L 1987 *Solid-State Electron.* **30** 693
[33] Sabbah A J and Riffe D M 2002 *Phys. Rev.* B **66** 165217
[34] Gallant M I and van Driel H M 1982 *Phys. Rev.* B **26** 2133
[35] Baskin L M, Lvov O I and Fursey G 1977 *Phys. Status Solidi* **42** 757
[36] Sokolowski-Tinten K and von der Linde D 2000 *Phys. Rev.* B **61** 2643
[37] Sernelius B E 1989 *Phys. Rev.* B **40** 12438
[38] Fischetti M V, Ren Z, Solomon P M, Yang M and Rim K 2003 *J. Appl. Phys.* **94** 1079
[39] Brattain W H and Shockley W 1947 *Phys. Rev.* **72** 345

[40] Kaiser A, Rethfeld B, Vicanek M and Simon G 2000 *Phys. Rev.* B **61** 11437
[41] Flubacher P, Leadbetter A J and Morrison J A 1959 *Phil. Mag.* **4** 273
[42] Mingo N, Yang L, Li D and Majumdar A 2003 *Nano Lett.* **3** 1713
[43] Harrison W A 1956 *Phys. Rev.* **104** 1281
[44] Gonzalez B, Palankovski V, Kosina H, Hernandez A and Selberherr S 1999 *Solid-State Electron.* **43** 1791
[45] Yoffa E J 1981 *Phys. Rev.* B **23** 1909
[46] Silaeva E P, Shcheblanov N S, Itina T E, Vella A, Houard J, Sevelin-Radiguet N, Vurpillot F and Deconihout B 2012 *Appl. Phys.* A (Online First, doi:10.1007/s00339-012-7189-7)
[47] Da Costa G, Vurpillot F, Bostel A, Bouet M and Deconihout B 2004 *Rev. Sci. Instrum.* **76** 013304
[48] Miller M K and Russell K F 2007 *Ultramicroscopy* **107** 761
[49] Forbes R G 1995 *Appl. Surf. Sci.* **87–88** 1
[50] Vella A, Deconihout B, Marrucci L and Santamato E 2007 *Phys. Rev. Lett.* **99** 046103
[51] Tsong T T 1984 *Phys. Rev.* B **30** 4946
[52] Kingham D R 1982 *Surf. Sci.* **116** 273